Clinical Neurophysiology 156 (2023) 207–219

Contents lists available at ScienceDirect

Clinical Neurophysiology

journal homepage: www.elsevier.com/locate/clinph

Infra-slow fluctuations in cortical potentials and respiration drive fast cortical EEG rhythms in sleeping and waking states

Tommi Väyrynen [a,b,c,*], Heta Helakari [a,b,c], Vesa Korhonen [a,b,c], Johanna Tuunanen [a,b,c], Niko Huotari [a,b,c], Johanna Piispala [b,c,d], Mika Kallio [b,c,d], Lauri Raitamaa [a,b,c], Janne Kananen [a,b,c,d], Matti Järvelä [a,b,c], J. Matias Palva [e,f,g,1], Vesa Kiviniemi [a,b,c,h,1]

[a] Oulu Functional NeuroImaging (OFNI), Department of Diagnostic Radiology, Oulu University Hospital, Oulu 90029, Finland
[b] MIPT group to: Research Unit of Health Sciences and Technology (HST), Faculty of Medicine, University of Oulu, Oulu 90220, Finland
[c] Medical Research Center (MRC), Oulu 90220, Finland
[d] Clinical Neurophysiology, Oulu University Hospital, Oulu 90220, Finland
[e] Department of Neuroscience and Biomedical Engineering, Aalto University, 02150 Espoo, Finland
[f] Neuroscience Center, Helsinki Institute of Life Science, University of Helsinki, Finland
[g] Centre for Cognitive Neuroimaging, University of Glasgow, United Kingdom
[h] Biocenter Oulu, Faculty of Biochemistry and Molecular Medicine, University of Oulu, Oulu 90220, Finland

HIGHLIGHTS

- Infra-slow fluctuations (ISF) and respiration are both coupled with fast neuronal oscillation amplitudes.
- ISF and respiration drive amplitude dynamics of fast oscillations in sleeping and waking states, with different contributions.
- Our findings suggest these slow physiological phases have significant role in determining the dynamics of cortical oscillations.

ARTICLE INFO

Article history:
Accepted 23 October 2023
Available online 3 November 2023

Keywords:
EEG
Sleep
Respiration
Slow oscillation
Modulation
Coupling

ABSTRACT

Objective: Infra-slow fluctuations (ISF, 0.008–0.1 Hz) characterize hemodynamic and electric potential signals of human brain. ISFs correlate with the amplitude dynamics of fast (>1 Hz) neuronal oscillations, and may arise from permeability fluctuations of the blood–brain barrier (BBB). It is unclear if physiological rhythms like respiration drive or track fast cortical oscillations, and the role of sleep in this coupling is unknown.

Methods: We used high-density full-band electroencephalography (EEG) in healthy human volunteers (N = 21) to measure concurrently the ISFs, respiratory pulsations, and fast neuronal oscillations during periods of wakefulness and sleep, and to assess the strength and direction of their phase-amplitude coupling.

Results: The phases of ISFs and respiration were both coupled with the amplitude of fast neuronal oscillations, with stronger ISF coupling being evident during sleep. Phases of ISF and respiration drove the amplitude dynamics of fast oscillations in sleeping and waking states, with different contributions.

Conclusions: ISFs in slow cortical potentials and respiration together significantly determine the dynamics of fast cortical oscillations.

Significance: We propose that these slow physiological phases play a significant role in coordinating cortical excitability, which is a fundamental aspect of brain function.

Abbreviations: BBB, blood–brain barrier; BOLD, blood oxygen level dependent; CSF, cerebrospinal fluid; dPTE, directed phase transfer entropy; $ETCO_2$, end-tidal carbon dioxide; fbEEG, full-band electroencephalogram; FDR, false discovery rate; fMRI, functional magnetic resonance imaging; ICA, independent component analysis; ISF, infra-slow fluctuations; MEG, magnetoencephalography; MREG, magnetic resonance encephalography; NREM, non-rapid eye movement; PAC, phase-amplitude coupling; PLV, phase locking value; PTE, phase transfer entropy.

* Corresponding author at: Oulu Functional NeuroImaging (OFNI), Department of Diagnostic Radiology Oulu University Hospital, Kajaanintie 50, 90220 Oulu, Finland.
E-mail address: tommi.vayrynen@oulu.fi (T. Väyrynen).

[1] Authors had equal contributions.

https://doi.org/10.1016/j.clinph.2023.10.013
1388-2457/

1. Introduction

An increasing focus has been directed toward establishing the link between slow physiological signals and neuronal rhythms as recorded using various neuroimaging modalities. Quasiperiodic infra-slow fluctuations (ISF_{EEG}, 0.008–0.1 Hz) (Hughes et al., 2011; Palva and Palva, 2012; Vanhatalo et al., 2004) comprise the strongest signal in full-band electroencephalography (fbEEG) (Niedermeyer et al., 2011). In awake state, the ISF_{EEG} are correlated with statistically independent ISFs in connected networks of the blood-oxygenation-level dependent (BOLD) signal during functional magnetic resonance imaging (fMRI) (Hiltunen et al., 2014; Leopold et al., 2003). ISF_{EEG} are also coherent with near infrared spectroscopy measurements of brain oxygenation levels (Nikulin et al., 2014). Magnitude of ISFs in the EEG (Marshall et al., 1998, 1996) and the neurovascular BOLD signal (Fukunaga et al., 2006; Fultz et al., 2019, Helakari et al., 2022) are greater during sleep than in the awake state.

The ISFs are commonly high-pass filtered in conventional EEG setups, as they have been thought to arise from non-neuronal sources such as alterations in cerebral blood flow (CBF) (Besson et al., 1970; Held et al., 1964; Tschirgi and Taylor, 1958). Recent studies with animal models (Nita et al., 2004) and humans (Kiviniemi et al., 2017) show that the dynamics of blood–brain barrier (BBB) permeability could be a major contributor to the ISF_{EEG} signal in addition to blood volume changes. ISF_{EEG} have been suggested to couple with cortical excitability during wakefulness (Monto et al., 2008) and sleep (Vanhatalo et al., 2004).

In addition to the relationship between ISF and fast brain rhythms, there is also a link between EEG respiration related activity ($RESP_{EEG}$) and fast neuronal changes. For example, intracranial electrophysiological studies with mice linked respiration and neuronal changes, claiming that respiratory phase modulated the power of gamma oscillations (Biskamp et al., 2017; Ito et al., 2014; Yanovsky et al., 2014). In humans, the respiratory cycle also correlates with corticospinal excitability (Li and Rymer, 2011), and sensory perception (Flexman et al., 1974). Subsequent human intracranial EEG studies showed that oscillations extending from theta to gamma frequencies were modulated in amygdala and hippocampus by respiration, with additional associations emerging in various cortical and subcortical sites in epileptic patients (Herrero et al., 2018; Zelano et al., 2016). Also, fMRI study of patients with epilepsy found increased respiratory power and synchrony (Kananen et al., 2022, 2020). Finally, findings from EEG and magnetoencephalography (MEG) studies conducted in healthy individuals have indicated that spontaneous brain activity is phase-locked and modulated by respiration during wakefulness (Kluger and Gross, 2021; Perl et al., 2019). Additionally, both the ISF and respiratory phase have shown correlations with behavioral performance in a stimulus-detection in humans, suggesting that the EEG signal derives functionally significant contributions from these slow, non-neuronal physiological signals (Johannknecht and Kayser, 2022; Monto et al., 2008).

While it is true that causality can sometimes be inferred from the timing of events, relying solely on the time difference between two events to infer causality can be problematic. There may be other factors, such as common underlying causes, that could explain the observed time difference. Although some studies have used non-directional correlative metrics to infer causal effects, these approaches are not generally reliable for establishing causality. In order to determine the direction of the studied interactions, we utilized phase transfer entropy (PTE) (Lobier et al., 2014). This novel metric offers a sensitive way to assess the direction of information flow. PTE is similar to the well-known Granger causality, and when dealing with Gaussian variables, these two measures are, in fact, equivalent. EEG signals are always linear mixtures of neural and non-neural sources, which are volume conducted to the scalp, and are generally highly correlated with each other (Nunez et al., 1997). PTE is a robust connectivity estimator for large-scale EEG scalp recordings, even in the presence of noise and linear mixing (Lobier et al., 2014). It can provide frequency-specific information about the direction of causality between phase time-series, independent of shared history.

Altogether, multiple lines of evidence suggest a connection between slow physiological phases and fast (>1 Hz) neural potentials (Kluger and Gross, 2021; Monto et al., 2008; Vanhatalo et al., 2004). However, the causal nature of the ISF coupling as well as its spatial distribution, remains undetermined. With respiration, directionality of the coupling along with effect of sleep call for more fundamental investigation. In this regard, our first objective in the present study was to assess how the low frequency characteristics of the EEG alter in the transition from waking to sleep. Second, we asked whether the ISFs (ISF_{EEG}) and respiration ($RESP_{EEG}$) induced EEG signals arise as a "byproduct" of emergent slow dynamics (Palva et al., 2013) of fast neuronal oscillations, or rather play a causal role in modulating the fast neuronal oscillations *per se*. To further elucidate the underlying mechanistic basis of these interactions, our final objective was to uncover whether coupling between fast neuronal processing and non-neuronal slow processes would be altered during non-rapid eye movement (NREM) sleep. To test these conjectures, we assessed spectral power, phase-amplitude coupling, and directional drive between ISF_{EEG} and fast oscillations in human brain using a 256-channel EEG during wakefulness and sleep. Our results show that slow physiological oscillation phases both couple and drive fast neurophysiological rhythm amplitudes across awake and sleep states in healthy human volunteers.

2. Methods

2.1. Experimental setting

The study received approval from the Regional Ethics Committee of the Northern Ostrobothnia Hospital District. Written informed consent was obtained from all participants in accordance with the principles outlined in the Declaration of Helsinki. All the subjects were healthy non-smokers, with no continuous medication, neurological or cardio-respiratory diseases.

In our previous research using multimodal measurement techniques, we observed a dynamic relationship between brain cortex BOLD and ISF_{EEG} signals (Keinänen et al., 2018; Korhonen et al., 2014). The sleep induced changes of ultrafast BOLD signal spectral power and entropy have been recently released in a publication by (Helakari et al., 2022) in the same group of participants. However, due to the complexity of analyzing ISF and respiratory band information across the entire brain using advanced phase analytics, our current study focused only on assessing the effects of sleep on multiband EEG. With the causality measures established in this study, our future goal is to integrate BOLD, ISF_{EEG}, and fNIRS data to comprehensively infer causal relationships in sleep-induced brain changes.

Thirty subjects were scanned twice in the study. One scanning session with eyes fixated on a cross was obtained at 4–6 PM on the day after a full night of sleep, and another scan starting at 7–9 AM followed upon a night of sleep deprivation. Generally, the awake scans were conducted prior to the sleep scans, specifically on Tuesdays and Wednesdays. Sleep deprivation scanning was car-

ried out on Saturdays. Both sets of scans were performed within one week, except for one subject who had a two-week gap between the scans. Additionally, there was one instance where a sleep deprivation scan occurred on Sunday. Each session consisted of two consecutive scans each lasting 10–15 minutes. Sleep deprivation was intended to enable the subjects to enter more quickly a deeper sleep state during the recordings (Horovitz et al., 2009; Kaufmann et al., 2006). Subjects were instructed not to drink any caffeinated beverages in the four hours before the awake resting state scan, and were requested to abstain for eight hours prior to the sleep deprivation scans. Consumption of alcohol was also prohibited in these intervals. Three subjects who, according to their sleep scores, did not fall asleep during the sleep deprived session, were excluded from the study (Table S1). Three subjects were also excluded due to suspicion of sleep apnea. Recordings were also disregarded in cases of insufficient signal quality. The resulting sizes of the groups were 21 awake (mean ± SD, age 29.2 ± 6.8 years, 8 females) and 21 (28.4 ± 6.3 years, 11 females) sleep subjects. We recorded the fbEEG recordings using the GES 400 (Electrical Geodesics) system, which consisted of a direct current (DC)-coupled amplifier (Net Amps 400) and a high-density 256-channel net (HydroCel Geodesic Sensor MR net). All the systems were compatible with magnetic resonance imaging (MRI). We used a sampling rate of 1 kHz (250 Hz for three sleep and five awake subjects, due to human error). Our recording setup used the "Cz" electrode as the reference channel. Prior to the recordings, signal quality and electrode impedances were carefully examined. End-tidal carbon dioxide ($ETCO_2$) was also measured in synchrony with the EEG and fMRI.

2.2. Data preprocessing

We used template subtraction (Allen et al., 2000) implemented in Brain Vision Analyzer (v.2.1, Brain Products) to remove gradient artifacts arising from MRI gradient switching. Template subtraction was also used to remove ballistocardiographic artefacts (Allen et al., 1998). The remaining signal processing and calculations were designed and performed in Matlab (v.R2018b-2019b, MathWorks). First, we segmented the EEG recordings to a matching duration of ten minutes. To mitigate stable baseline drift caused by conductivity changes between the electrode and skin, we removed linear trends (Huigen et al., 2002), which are known to affect the performance of various pre-processing steps.

We used amplitude threshold and visual confirmation to determine bad channels for awake (0–8, average 2.4 bad channels) and sleep (0–4, average 1.3 bad channels) measurements. We used independent component analysis (ICA) (FastICA (Hyvarinen, 1999)) along with principal component analysis dimension reduction (150 components) to transform datasets into independent components, in which artifactual ICs were identified and removed. Artifactual ICA components were detected using SASICA toolbox (Chaumon et al., 2015) for EEGLAB (Delorme and Makeig, 2004), based on autocorrelation of the components and correlation with electrooculogram channels. Focal components were also removed. Our primary focus here was on removing ocular components, which can also appear as low-frequency events (<1 Hz). During the awake scans, subjects were specifically instructed to maintain fixation on a cross, which is a known technique for reducing the occurrence of saccadic eye movements. To maximize the performance of ICA and minimize non-linearities, we employed a custom spike detection algorithm aimed at eliminating artificially generated spikes characterized by significantly high amplitudes. To address the gaps that arose as a result, we employed a two-phase process resembling inpainting (de Cheveigné and Arzounian, 2018). In the first phase, we interpolated the trend within the gaps, ensuring a smooth transition edges. Next, we utilized intact signal to generate real data mimicking injections, which was then added to the interpolated trend. This approach enabled a seamless transition with properties consistent with genuine data, as opposed to abrupt edges that would result from simply removing the artifactual segments. The previously identified bad channels were excluded from the ICA. Following that, spherical interpolation was applied to replace the excluded channels. Regarding referencing, the recordings were referenced to linked mastoid electrodes. These mastoid electrodes were positioned in close proximity to other electrodes however, they capture lower levels of brain activity. Recordings were sleep-scored manually by experienced clinical neurophysiologists (JP, MK) following American Academy of Sleep Medicine guidelines (Table S1).

2.3. Spectral analysis

We performed time–frequency spectral analysis (Fig. 1a) by employing wavelet convolution in the frequency domain, which offered faster computation in contrast to time domain. We used complex Morlet wavelets (Eq.1) together with mirrored time-series to mitigate the edge effects commonly arising in temporal filtering processes. Conventional Fourier transform assumes signal stationarity, meaning that statistics of the signal, including mean, variance and frequency structure of the signal, do not change over time (Cohen, 2014). However, the stationarity assumption is violated by long EEG data, leading to decreased accuracy of frequency estimates. This, along with the potential to generate time-resolved frequency representations with computational efficiency, led us to use wavelets. Fourier transform and Morlet wavelets both employ sine waves as kernels, but in the latter case the sine wave is not the full length of the recording and is tapered by a Gaussian window (Cohen, 2014). The Gaussian window is preferred over a rectangular window due to its smooth transition edges, whereas the sharp

Fig. 1. Effect of sleep on oscillation power and phase-amplitude coupling (PAC) with cortical rhythms. a) The relative amplitude of EEG signals is shown on a logarithmic frequency scale. Shadings around the mean lines represent standard deviations of awake (red) and sleep (blue) states. The width of the solid lines indicates statistical significance ($p < 0.05$) in ascending order of rank: no statistical significance, permutation tested, permutation test + maximum statistics correction. Topography plots of the relative power difference (awake-sleep) in infra-slow fluctuations (ISF < 0.01 Hz), slow-wave (0.2–2 Hz) and fast frequency bands. b) The top section provides an illustration of PAC using an EEG trace. The full-band EEG trace is initially filtered into low- and high-frequency signals separately. The high-frequency signal is then processed by extracting its envelope and further filtering it to the low frequency range. Both signals have their phases extracted, allowing for the application of phase-based metrics. Bottom left: Median phase-locking values (PLV) taken over electrodes. Asterisks indicate statistically significant differences (adjusted $p < 0.05^{*}$, 0.01^{**}, 0.001^{***}) in coupling strength between awake and sleep states. Gray lines connect paired subjects. Bottom right: Box plot describing the number of significantly coupled electrodes per subject, scaled to percentiles. The fast frequency bands are denoted by Greek letters. c) The difference in average PLV (awake-sleep) is shown. Significant values after permutation testing ($p < 0.05$) are highlighted using a p-value mask. A stricter significance criterion using maximum statistic correction ($p < 0.05$) is visualized with yellow circles. d) Probability estimates of the average phase difference in radians between ISF phase and fast rhythm phases. The probability estimate was combined over all fast frequency bands. Channels on the y-axis are sorted in ascending order following the median phase difference. Topography plots display the median phase difference taken over the fast bands and subjects.

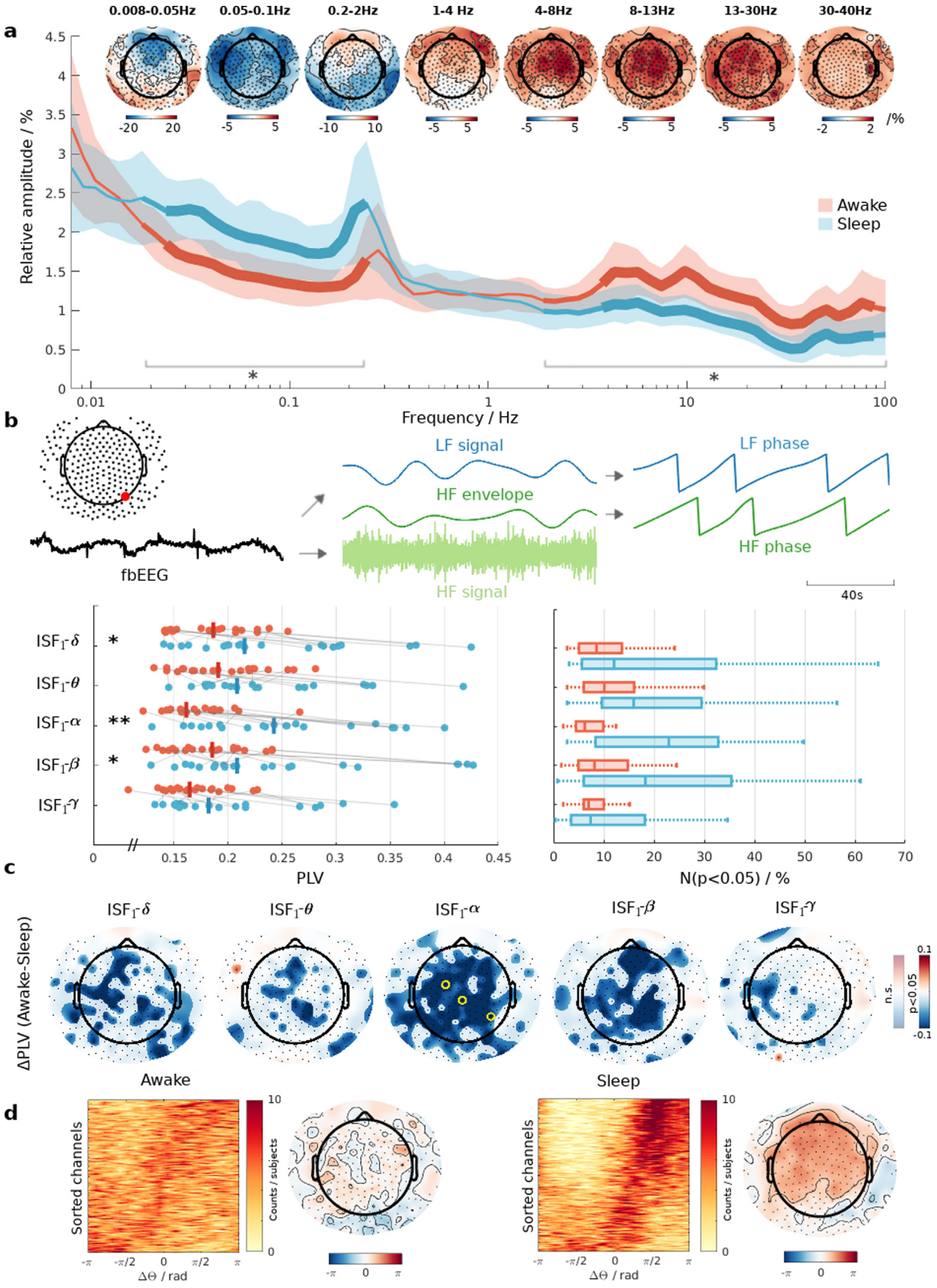
a
0.008-0.05Hz
0.05-0.1Hz
0.2-2Hz
1-4 Hz
4-8Hz
8-13Hz
13-30Hz
30-40Hz
/%
Relative amplitude / %
Awake
Sleep
Frequency / Hz
b
fbEEG
LF signal
HF envelope
HF signal
LF phase
HF phase
40s
ISF1-δ
ISF1-θ
ISF1-α
ISF1-β
ISF1-γ
PLV
N(p<0.05) / %
c
ΔPLV (Awake-Sleep)
Awake
Sleep
n.s.
p<0.05
d
Sorted channels
Counts / subjects
ΔΘ / rad

edges in simple rectangular windowing gives rise to artifactual ripple effects (Cohen, 2019).

In this analysis, we selected 70 frequency points within a logarithmic frequency range spanning from 0.008 to 100 Hz. We kept the number of wavelet cycles constant (N = 7), which controls the temporal and frequency precision (Eq. 2). The time–frequency power estimates were obtained by calculating the squared magnitude of the convolution results. To categorize the time–frequency power estimates into epochs of wakefulness and sleep (N1-N3), we utilized sleep scores as a reference. These sleep scores served to discard awake epochs from the sleep samples, and vice versa, thus affording even more accurate spectral estimates. We then averaged over the time dimension and then formulated power to relative amplitudes (Eq. 3), thus reducing individual variability in power. To compute the relative band power topographies, we calculated the sum of power within specific frequency bands. This summed power was then divided by the total power across all recorded frequencies. The resulting relative expression answers the question of how much of the total power is attributed to a particular frequency band.

2.4. Phase-amplitude coupling

To ensure full coverage of ISF frequencies without overlap with respiration frequencies, we selected ISF frequencies ranging from 0.008 Hz to 0.1 Hz. We separated two distinct ISF bands ($ISF_{1\text{-}EEG}$: 0.008–0.05 Hz & $ISF_{2\text{-}EEG}$: 0.05–0.1 Hz), each extracted using finite impulse response (FIR) filters. For the design of these FIR bandpass filters, we used Hamming window function and determined the filter kernel length based on one cycle of the lowest frequency of interest. Since edge artifacts are prominent particularly during temporal filtering of the lowest frequencies, we used a mirroring technique to extend the time-series $x(n), (n = 1, ..., N)$ at both ends. This allowed us to create buffer zones around the signals, which were later discarded. Additionally, to avoid potential phase distortions and offsets that can occur with conventional one-way filtering methods, we utilized zero-phase filtering. This way the signals were filtered in the forward and reverse directions $x_{ISF}(n)$, effectively reducing any phase distortions or offsets. As for the ISF, we designed FIR bandpass filter for the fast frequency bands (delta: 1–4 Hz, theta: 4–8 Hz, alpha: 8–13 Hz, beta: 13–30 Hz, gamma: 30–40 Hz). To gain even sharper frequency response, we increased the filter kernel length to six times the period of the lowest frequency. We then applied zero-phase filter to produce $x_{fast}(n)$ signals.

Phase-amplitude coupling refers to a type of cross-frequency coupling in which the phase of a slower frequency is coupled to the amplitude of a faster rhythm. Here, we evaluated phase locking value (PLV) (Lachaux et al., 1999), to quantify the strength of coupling between the phase of the ISF and the amplitudes of the faster oscillations. Our methodology for assessing this coupling was based on previous studies conducted by (Monto et al., 2008; Palva et al., 2005; Vanhatalo et al., 2004). First, to acquire the instantaneous phase time-series of the ISF we calculated analytical signals $z_{ISF}(n)$ (Eq.4) using Hilbert transform. The phase was extracted as an argument of the analytical signal $\theta_{ISF} = arg(z_{ISF}(n))$. For fast frequency bands, Hilbert transform was applied twice: first to compute Hilbert amplitude envelope as a complex magnitude of the analytical signal $a(n) = |z_{fast}(n)|$, which was then filtered to ISF bands with same FIR filter as described before. Since the temporal resolution required for phase-amplitude coupling analysis is dependent on the slower ISF phase, we performed down-sampling of the signals to 3 Hz. This resampling allowed for faster computation while still capturing the dynamics of the ISF phase. We then applied second Hilbert transform to the envelopes $A_{fast}(n)$ to compute instantaneous phase as an argument of the analytical signal $\theta'_{fast} = arg(z_{A_{fast}}(n))$. Finally, we calculated 1:1 phase locking between θ_{ISF} and θ'_{fast} to quantify the phase-amplitude coupling. We calculated PLV (Eq.5) for each electrode and combinations of ISF and fast frequency bands. We present a diagram of the workflow in Supplementary Figure S1.

The respiratory frequency phase-amplitude coupling with fast oscillations was calculated following same principles as with ISF. $ETCO_2$ recordings were used to assess individual respiration frequencies which were recorded simultaneously with the EEG measurements. We calculated spectrograms for the $ETCO_2$ signals with short-time Fourier transform. We used 50 second Hamming-tapered windows and 50 % overlap with each other. The peaks of the spectra, representing dominant respiration frequencies, were then used for defining the center frequency of complex Morlet wavelets (N = 5). For three subjects in the awake group and two subjects in the sleep group we used median frequency of the group for calculations, as $ETCO_2$ signals were not recorded. We implemented the wavelet convolution in frequency domain as before to perform filtering to the respiration frequencies. For faster frequency bands the Hilbert amplitude envelopes were computed from analytical signals and then filtered to respiratory frequency. Second Hilbert transform was then utilized to extract instantaneous phase time-series and phase-amplitude coupling was quantified again as phase locking between θ_{RESP} and θ'_{fast}.

2.5. Phase transfer entropy

To resolve the yet unanswered question concerning direction of the drive between the slow and fast rhythms we used recent information theory-based measure PTE (Lobier et al., 2014). It is an effective connectivity measure describing information flow between two phase time-series. PTE results can be interpreted as if the observation of source signal helps to predict the transitions of the target signal. It is derived from real-valued transfer entropy and is also used in similar way, with a distinction that is applied to instantaneous phase signals.

We used the same instantaneous phase time-series θ_{slow} and θ'_{fast} as with PLV calculations, now with 125 Hz sampling. First, we utilized the state space transition to generate discrete probability distributions, and from these distributions, we computed Shannon entropies. Reduction in uncertainty of the variable is described by Shannon's entropy, which in this context defines the information content. To determine the adequate number of bins for the calculations we used Scott's choice (Scott, 1979) (Eq. 6). In order to calculate PTE as described in (Eq.7) we first had to compute the joint and individual entropy probabilities in equations 8–10. To express information in units of bits, we used a logarithm base of 2 (Bossomaier et al., 2016; Timme and Lapish, 2018). Subsequently, we transformed the PTE values into their directional form, known as dPTE (Eq.11), where the sign of the metric indicates the direction of net information flow. While performing the PTE analysis, we made an *a priori* assumption of the analysis lag, setting it to one cycle of the slow phase. However, PTE values are not sensitive to the analysis lag, allowing accurate estimate of connectivity over a wide range of delays (Lobier et al., 2014).

2.6. Statistical analysis

No statistical methods were used to pre-determine sample sizes. For spectral estimate (Fig. 1a), we constructed the null hypothesis distribution using a nonparametric permutation test, where we iteratively shuffled the condition labels (groupwise difference) over the subjects 10,000 times. For each frequency point, our null hypothesis held that wakefulness and sleep have an equal

contribution on spectral power (two-tailed). We then transformed this distribution of test statistics generated under the null hypothesis to standard Z values (Eq.12), from which we obtained the p-value by assessing its position on a Gaussian probability density function. We addressed the multiple comparison problem using a maximum statistic correction. In each iteration, we gathered the maximum and minimum values of the differences and used them to construct null distributions. These null distributions were then used to determine the statistical significance ($p < 0.05$), of maximum statistic correction. The significance thresholds were then given by 2.5th and 97.5th percentiles (two-tailed). Similarly, we used a nonparametric permutation test by shuffling the condition labels over subjects for average PLV difference topographies and dPTE topographies (Fig. 1c, 2c, 3c, 3f). Here, we tested each electrode with the null hypothesis that PLV and dPTE are not affected by change in vigilance state (two-tailed). As before, we permuted condition labels 10,000 times to generate the distribution of test statistics under the null hypothesis, from which the significance could be determined (Eq.12). We then used maximum statistic correction (two-tailed) to take into account the multiple comparisons problem, and extracted the statistical significance ($p < 0.05$) over the 2.5th to 97.5th percentile range.

We performed groupwise comparisons for the median PLV taken over electrodes using Wilcoxon rank sum test (Figures: 1b, left & 3b, left). Our null hypothesis held that vigilance does not affect PLV (two-tailed). We used false discovery rate (FDR) correction (Benjamini and Hochberg, 1995) to decrease the false discovery rate otherwise arising from multiple comparisons. Similarly, for $ETCO_2$ (Fig. 3a) we used the two-tailed Wilcoxon rank sum test, with null hypothesis that median frequency of respiration does not change with respect to arousal state.

In order to evaluate the significance of phase-amplitude coupling on the subject level (Fig. 1b, right & 3b, right), we employed a method of time shifted surrogate data (Arnulfo et al., 2020; Lachaux et al., 1999; Theiler et al., 1992). Surrogate data reflects properties of the real signal as the autocorrelation structure is preserved, but effectively destructing correlations between two signals. First, we constructed the surrogate data by splitting the phase of time-series $x(t = 1,\ldots,T)$ from a random time-point k into $x_1 = x(1,\ldots,k)$ and $x_2 = x(k,\ldots,T)$, thus constructing the surrogate time-series $x_s = [x_2,x_1]$. We built the surrogate PLV null distribution, using 100 surrogate time-series. Using surrogate distribution, we accepted or rejected the null hypothesis stating that PLV comes from the null distribution (Eq.13). In all of the statistical tests, the adjusted significance threshold was set as $p < 0.05$ for rejection of the null hypothesis.

We used one sample sign test to assess whether the median dPTE differed from zero, which would indicate the presence of directionality in the phase-amplitude interaction. To correct for false positives, we adjusted the p-values using FDR-correction (Benjamini-Hochberg) with 95 % confidence level (Fig. 2b & 3e). For groupwise two-tailed comparisons, we used two sample Wilcoxon rank sum to test if the medians of awake and sleep groups were equal (Fig. 2b & 3e). Similar to previous tests, we used FDR-correction to obtain adjusted p-values with 95 % confidence level ($p < 0.05$). We utilized previously calculated z-values to estimate the effect sizes (η^2) as defined by the equation: $\eta 2 = (Z/\sqrt{N})^2$, where the total sample size is denoted by N (Fritz et al., 2012).

3. Results

3.1. Infra-slow frequency power increases during sleep

We hypothesized that EEG low frequency power should increase in sleep in concert with previously described increases in ISF BOLD signal power. To determine how the frequency characteristics of the electrophysiological signal change in NREM sleep, we used spectral analysis to assess the differences in the power in infra-slow and higher frequency bands between sleep and awake states (Fig. 1a). During sleep, whole head spectral power was higher (2-sample permutation test) in the ISF_{EEG} and $RESP_{EEG}$ frequency band between 0.02–0.25 Hz ($\overline{\Delta RA}$ = -0.519 %, $p < 0.05$, $\bar{Z}$=-3.687), and on the other hand was decreased in frequencies above 1.9 Hz ($\overline{\Delta RA}$ = 0.328 %, $p < 0.05$, $\bar{Z}$=3.544). Slow-wave (0.2–2 Hz) EEG topography revealed increased spectral power during sleep, which was evident throughout most of the cortical surface, except for the frontal electrodes. Consistent with our hypothesis, the power of the ISF showed significant enhancement across broad cortical regions during sleep, particularly in the frontal areas. Conversely, there was a decrease in high-frequency power when transitioning to sleep, indicating a shift in the dominant cortical oscillation power from high to low frequencies during NREM sleep.

3.2. Sleep increases the synchronization between infra-slow fluctuations and fast cortical amplitudes

We next tested the prediction that the coupling between the physiological slow brain fluctuations and neuronal oscillations would increase in sleep. To specifically investigate the connection between the phase of ISF and the amplitudes of fast oscillations, we utilized a phase-amplitude coupling estimator that relied on the PLV (Vanhatalo et al., 2004). This estimator allows for the identification of phase-amplitude coupling effects linked to specific ISF frequencies in the amplitude signal. The oscillation period of ISFs exhibits considerable variability, ranging from as short as ten seconds to well over a hundred seconds. This poses a challenge since phase is a characteristic of narrow-band signals, and thus phase-based metrics need to be computed specifically for narrow-band signals. To address this issue, we divided the ISF_{EEG} data into two distinct frequency ranges: $ISF_{1\text{-}EEG}$ (0.008–0.05 Hz) and $ISF_{2\text{-}EEG}$ (0.05–0.1 Hz). It is worth noting that ISFs are commonly observed around 0.02 Hz in both mice and humans (Watson, 2018). Therefore, we present the results related to $ISF_{2\text{-}EEG}$ in the Supplementary section (Figures S2 & S3).

In line with our hypothesis, the phase-amplitude coupling between $ISF_{1\text{-}EEG}$ phase and the fast amplitudes was increased in sleep (mean ± SD, $\overline{PLV}$=0.211 ± 0.022) compared to awake ($\overline{PLV}$ = 0.178 ± 0.014) recordings (Fig. 1b, left). Groupwise differ-

Fig. 2. The phase of infra-slow fluctuations (ISF_1) drives amplitudes of fast cortical oscillations. a) The box plot illustrates phase transfer entropy (PTE) between ISF_1 and fast amplitudes in both directions: ISF->fast (solid line) and fast->ISF (dashed line) for wakefulness (red) and sleep (blue). The fast frequency bands are denoted by Greek letters and the units are in bits. b) The probability density estimate depicts the average directional PTE (dPTE). As dPTE is a directional metric, the net prediction direction changes upon a sign change. Asterisks indicate statistical significance (adjusted $p < 0.05^*$, 0.01^{**}, 0.001^{***}): colored asterisks denote significant non-zero drive in one-sample tests, while black asterisks represent two-sample groupwise comparisons. c) The topography displays the average dPTE topography for awake (top), sleep (middle), and the difference (bottom). The difference topography is overlaid with a significance mask (permutation testing, $p < 0.05$). Electrodes exhibiting significance after maximum statistics correction ($p < 0.05$) are highlighted with yellow circles.

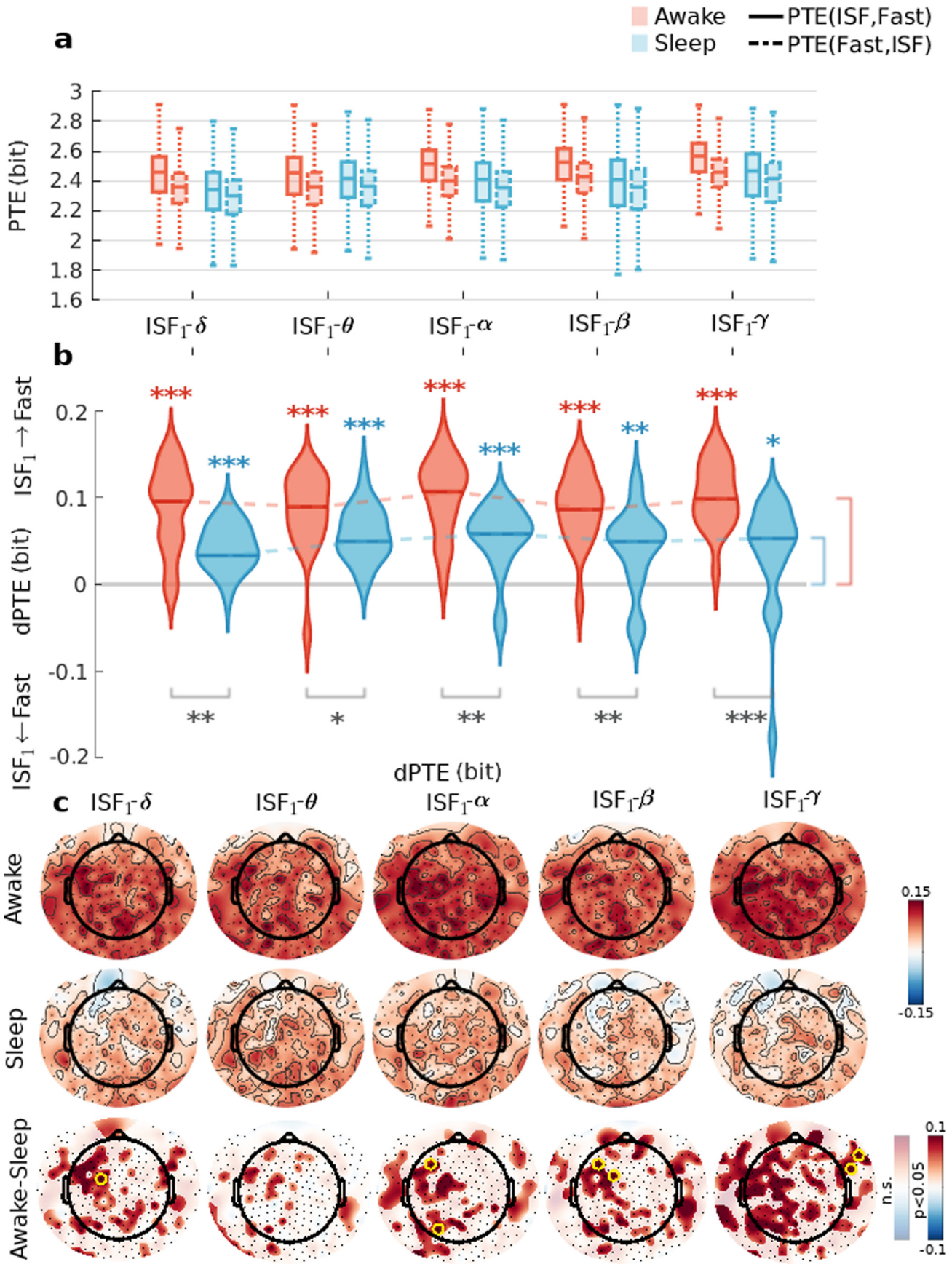
a
Awake
Sleep
PTE(ISF,Fast)
PTE(Fast,ISF)
PTE (bit)
3
2.8
2.6
2.4
2.2
2
1.8
1.6
ISF1-δ
ISF1-θ
ISF1-α
ISF1-β
ISF1-γ
b
ISF1 → Fast
dPTE (bit)
ISF1 ← Fast
0.2
0.1
0
-0.1
-0.2
***
**
*
dPTE (bit)
c
ISF1-δ
ISF1-θ
ISF1-α
ISF1-β
ISF1-γ
Awake
Sleep
Awake-Sleep
0.15
-0.15
0.1
n.s.
p<0.05
-0.1

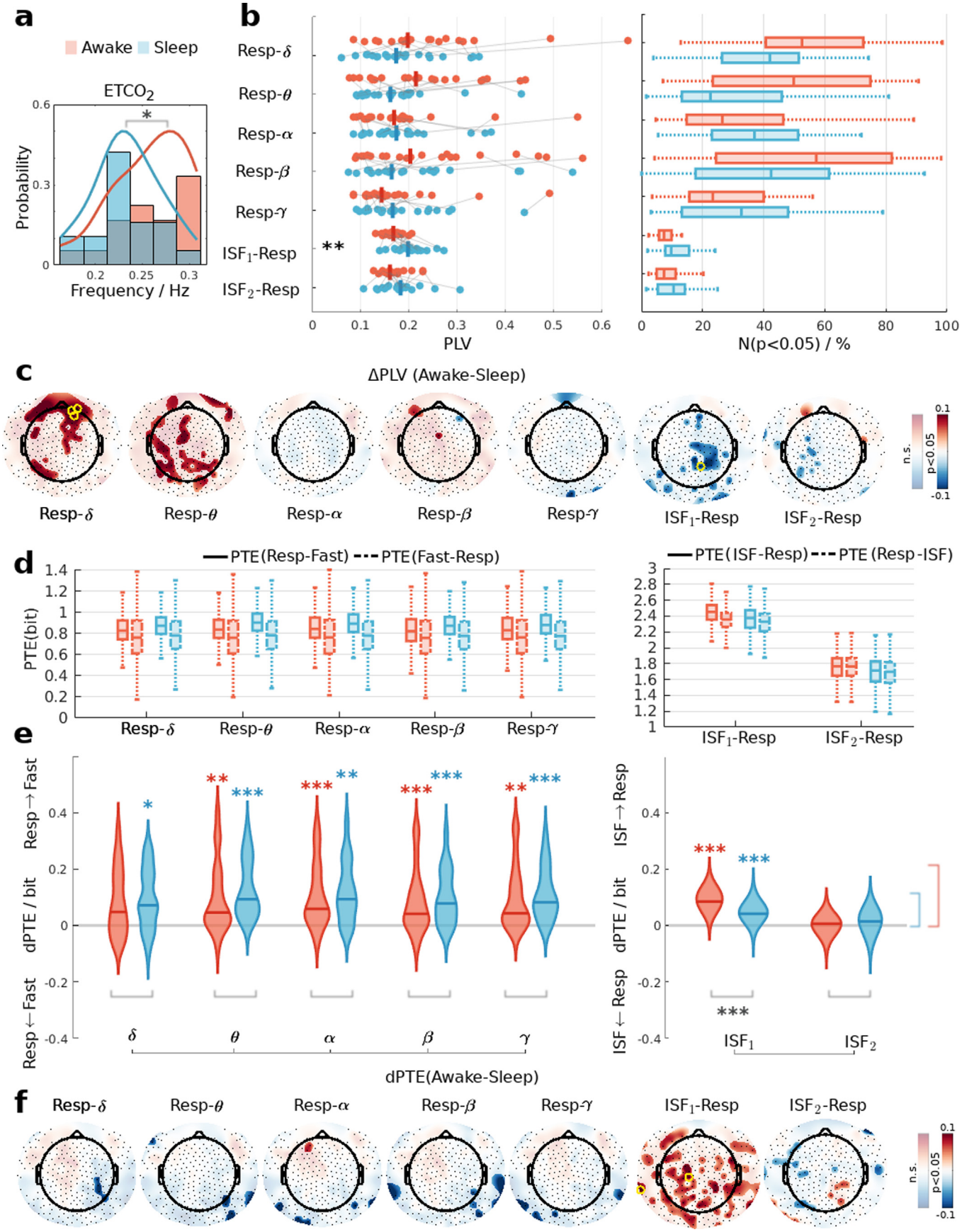
a
Awake
Sleep
ETCO2
Probability
Frequency / Hz
b
Resp-δ
Resp-θ
Resp-α
Resp-β
Resp-γ
ISF1-Resp
ISF2-Resp
PLV
N(p<0.05) / %
c
ΔPLV (Awake-Sleep)
n.s.
p<0.05
d
PTE(Resp-Fast)
PTE(Fast-Resp)
PTE(bit)
PTE(ISF-Resp)
PTE(Resp-ISF)
e
Resp→Fast
Resp←Fast
dPTE / bit
ISF→Resp
ISF←Resp
dPTE(Awake-Sleep)
f

ences in phase-amplitude coupling were significant (Wilcoxon rank sum, FDR) between the $ISF_{1\text{-}EEG}$ phase and the amplitude of delta (ΔPLV = -0.029, p_{adj} = 0.031, Z = -2.742), alpha (ΔPLV = -0.081, p_{adj} = 0.002, Z = -3.773), and beta (ΔPLV = -0.023, p_{adj} = 0.037, Z = -2.440) bands. The main emphasis of the differences were on central brain regions (Fig. 1c), where blue areas correspond to stronger PLV during sleep. Theta (ΔPLV = -0.017) and gamma (ΔPLV = -0.018) frequencies contained no significant differences. To evaluate the significance of coupling at the individual electrode level, we created a surrogate phase-locking value PLV distribution for each PLV by employing time-shifted surrogate data. We observed a similar trend in the PLV compared to the surrogates, as we did with the raw PLVs (Fig. 1b, right). The interquartile range for scalp electrodes showing significant ($p < 0.05$) phase-amplitude coupling was lower during wakefulness, with 5–15 % of channels exhibiting significant coupling effects. Similarly, during sleep, significant effects were observed in 5–35 % of electrodes.

To examine how the phase differences were distributed and whether they were coherent or not, we computed probability distributions for the average phase-amplitude coupling phase differences between the $ISF_{1\text{-}EEG}$ and fast oscillations and across all frequency bands (Fig. 1d & Figure S6). In wakefulness, the phase differences exhibited a relatively uniform distribution. During sleep, there was a substantial deviation in the pattern, primarily affecting frontal, parietal and central electrodes. This change was characterized by a clear inclination towards phase differences of $\pi/2$, which corresponded to the falling phase of the ISF cycle.

Collectively, these findings demonstrate a significant coupling between ISFs and the amplitude dynamics of fast neuronal oscillations in both awake and sleep states. Moreover, the strength and extent of this coupling are notably enhanced across the cortical surface during sleep.

3.3. Electrophysiological brain rhythms are predicted by infra-slow phase

We next asked whether there was any directed net drive, such that ISFs were driving the cortical amplitude fluctuations, rather than emerging as their consequence. To resolve this question, we.

calculated directed phase-amplitude coupling according to PTE between the phase of ISFs and the fast amplitudes. Upon assessing PTE in both possible directions of interaction (Fig. 2a), we found increased correlations for both directions and in all frequency bands during the awake state in comparison to sleep.

To identify whether the slow physiological or fast neuronal oscillations were the driver of the other, we configured PTE into a directional form. This approach revealed significant (Sign test, FDR) dPTE in all frequency bands during waking state: delta ($dPTE$ = 0.099 bit, $p_{adj} < 0.001$), theta ($dPTE$ = 0.093 bit, $p_{adj} < 0.001$), alpha ($dPTE$ = 0.110 bit, $p_{adj} < 0.001$), beta ($dPTE$ = 0.090 bit, $p_{adj} < 0.001$) and gamma ($dPTE$ = 0.103 bit, $p_{adj} < 0.001$) and likewise in sleep: delta ($dPTE$ = 0.038 bit, $p_{adj} < 0.001$), theta ($dPTE$ = 0.052 bit, $p_{adj} < 0.001$), alpha ($dPTE$ = 0.062 bit, p_{adj} = 0.001), beta ($dPTE$ = 0.053 bit, p_{adj} = 0.004) and gamma ($dPTE$ = 0.054 bit, p_{adj} = 0.014) (Fig. 2b). Of particular importance, the ISF phase demonstrated a higher degree of predictability for the fast rhythms than vice versa, thus providing compelling evidence that ISFs drive the amplitude dynamics of fast oscillations.

We found an increase in the median dPTE (Wilcoxon rank sum, FDR) during wakefulness ($\overline{dPTE}$ = 0.099 ± 0.008), in contrast to sleep ($\overline{dPTE}$ = 0.052 ± 0.009): delta (Δ $dPTE$ = 0.061 bit, p_{adj} = 0.003, Z = 3.195), theta (Δ $dPTE$ = 0.041 bit, p_{adj} = 0.018, Z = 2.616), alpha (Δ $dPTE$ = 0.048 bit, p_{adj} = 0.003, Z = 3.371), beta (Δ $dPTE$ = 0.037 bit, p_{adj} = 0.003, Z = 3.295) and gamma (Δ $dPTE$ = 0.049 bit, p_{adj} = 0.001, Z = 3.975). The magnitudes of dPTE remained stable across frequency bands, with minimal variation.

The lowered net drive during sleep, arose from decreased correlation in the direction from ISF to fast oscillations, and a simultaneous smaller decrease for the correlation in the opposite interaction direction (Fig. 2a). Scalp topography of the groupwise difference in dPTE (Fig. 2c) highlights the involvement of spatially overlapping regions, which was least evident in the theta frequency band. These findings establish the initial causal link between ISFs and the drive of fast cortical brain rhythms during wakefulness and sleep states.

In general, increased coupling should reflect increased information transfer between coupled oscillators (Ceguerra et al., 2011). We initially hypothesized that the increased phase-amplitude coupling observed during sleep (see Fig. 1b) was accompanied by lowered directional drive, since the phase difference tends to remain more constant with higher coupling (see Fig. 1d).

To test this conjecture, we quantified the relationship between phase locking strength and prediction magnitudes. This analysis revealed no linear correlation (awake: R^2 = 0.013, sleep: $R^2 = 4{*}10^{-5}$) between the two factors (Figure S4a).

We next asked whether the spectral power increase of ISF during sleep pointed to elevated autocorrelations, which might thereby underlie the changes in directional drive. However, the autocorrelations in terms of transfer entropy did not correlate with power (Wilcoxon rank sum, FDR) in ISF_1 (Z = -2.767, p_{adj} = 0.068), delta (Z = -1.233, p_{adj} = 0.610), theta (Z = -0.629, p_{adj} = 0.635), alpha (Z = -1.987, p_{adj} = 0.188), beta (Z = -2.038, p_{adj} = 0.188), gamma (Z = -0.730, p_{adj} = 0.621), and thus did not explain the difference in dPTE between arousal states (Figure S5), leading us to reject that hypothesis. Study utilizing the Kuramoto model, revealed that information transfer precedes coupling in such a way that decreased information transfer was observed before the oscillators were fully synchronized (Ceguerra et al., 2011). Thus, the decreased information transfer we observed with transition to sleep could indicate an approach towards such a stable state.

3.4. EEG respiratory phase is a driver for fast oscillation amplitudes

Our recent study showed that respiratory brain pulsations increase in the magnetic resonance encephalography (MREG) BOLD signal and overlap with fronto-parietal slow-wave electro-

Fig. 3. EEG respiratory frequency coupling and drive. a) Probability estimates of the individual respiratory frequencies taken from end-tidal CO_2. b) On the left, the scatter plot of phase-amplitude coupling showing median phase-locking values (PLV) between respiration frequency EEG signal ($RESP_{EEG}$) and fast frequency bands. Asterisks mark statistically significant differences (adjusted $p < 0.05^{*}$, 0.01^{**}, 0.001^{***}) in coupling strength between awake (red) and sleep (blue) states. Gray lines connect paired subjects. On the right, Box plot describing the number of significantly coupled electrodes per subject, scaled to percentiles. The fast frequency bands are denoted by Greek letters. c) Difference in average PLV (awake-sleep) overlaid with permutation testing ($p < 0.05$) p-value mask. A stricter significance criterion using maximum statistic correction ($p < 0.05$) is visualized with yellow circles. d) Phase transfer entropy (PTE) for both directions: $RESP_{EEG}$ ->fast (solid line) and fast-> $RESP_{EEG}$ (dashed line). The box contains the interquartile range (IQR) and whiskers 1.5*IQR in units of bits. On the left side, PTE between $RESP_{EEG}$ and fast frequency bands. On the right side, PTE between infra-slow fluctuations (ISF_{EEG}) and $RESP_{EEG}$ similarly for both directions (solid and dashed lines). e) The probability density estimate depicts the average directional PTE (dPTE). As dPTE is a directional metric, the net prediction direction changes upon a sign change. Asterisks indicate statistical significance: coloured asterisks denote significant non-zero drive in one-sample tests, while black asterisks represent two-sample groupwise comparisons. f) Topography shows median dPTE difference overlaid with a significance mask (permutation testing, $p < 0.05$). Electrodes exhibiting significance after maximum statistics correction ($p < 0.05$) are highlighted with yellow circles.

physiological changes in sleep (Helakari et al., 2022). The increased role of respiration in current research led us asking if respiration in EEG exhibits coupling with fast cortical amplitude oscillations, and if sleep has any effect on this association. To address this, we designed the same calculations as above with ISF, aiming to assess phase-amplitude coupling using subject specific individual respiration frequency EEG.

We found respiration frequencies to be higher (Wilcoxon rank sum, Z = 1.99, $p < 0.05$) during wakefulness (mean ± SD, $\bar{f}$=0.26 ± 0.041 Hz) compared to sleep ($\bar{f}$ = 0.23 ± 0.035 Hz) (Fig. 3a). The average level of phase-amplitude coupling was stronger during wakefulness ($\overline{PLV}$ = 0.185 ± 0.029) in contrast to sleep ($\overline{PLV}$ = 0.167 ± 0.006) (Fig. 3b), but we found no significant differences (Wilcoxon rank sum, FDR) between arousal states in any of the tested frequency bands. As before, we generated a surrogate PLV distribution for each PLV. Comparison with surrogate distributions showed that fast oscillation amplitudes are widely coupled with $RESP_{EEG}$ phase across the cortex. In the awake state recordings, the interquartile range of significantly ($p < 0.05$) coupled electrodes spanned from 15 % up to 80 %. However, during sleep, this range was narrower, ranging from 15 % to just 60 %. Even though whole head differences were non-significant, we found significant PLV differences for individual electrodes with the slowest delta band in frontal regions, and for theta frequencies in occipital areas (Fig. 3c).

As described above, to investigate further the directional drive between the $RESP_{EEG}$ and fast rhythms we quantified PTE and its directional form dPTE. Correlations were similar in both directions with respect to frequency band (Fig. 3d) with elevated PTE in the $RESP_{EEG}$ → fast direction. The baseline of $RESP_{EEG}$ PTE magnitudes was lower in comparison to the ISF-fast prediction. There was a robust dPTE between $RESP_{EEG}$ and fast brain rhythms (Fig. 3e) as indicated also by PTE. A net drive was present in almost every frequency band tested during wakefulness ($\overline{dPTE}$ = 0.049 ± 0.007), except for the delta rhythm, which was unaltered by sleep ($\overline{dPTE}$ = 0.085 ± 0.010). The slower $RESP_{EEG}$ drove fast oscillation amplitudes (Sign test, FDR) during wakefulness in all, except delta frequency band: delta ($dPTE$ = 0.051 bit, p_{adj} = 0.189), theta ($dPTE$ = 0.047 bit, p_{adj} = 0.002), alpha ($dPTE$ = 0.060 bit, $p_{adj} < 0.001$), beta ($dPTE$ = 0.041 bit, $p_{adj} < 0.001$) and gamma ($dPTE$ = 0.048 bit, p_{adj} = 0.002). In sleep, we found the same slow phase driven net directionality: delta ($dPTE$ = 0.073 bit, p_{adj} = 0.030), theta ($dPTE$ = 0.093 bit, $p_{adj} < 0.001$), alpha ($dPTE$ = 0.096 bit, p_{adj} = 0.002), beta ($dPTE$ = 0.080 bit, $p_{adj} < 0.001$) and gamma ($dPTE$ = 0.084 bit, $p_{adj} < 0.001$). Topographical mapping (Fig. 3f) separated occipital-parietal electrodes from the rest of the scalp, where there were only non-significant differences.

We also wanted to know if there was any interaction between the slow physiological ISF_{EEG} and $RESP_{EEG}$. With slower ISF_1 frequency range (0.008–0.1 Hz) we found increased (Wilcoxon rank sum, FDR) phase-amplitude coupling in sleep (ΔPLV = -0.03, p_{adj} = 0.008, Z = -3.245) (Fig. 3b). When PLVs were compared with surrogate distribution, we found that only 10 % of the electrodes were significantly coupled. Nonetheless, we still detected a significant drive (Sign test, FDR) directed from $ISF_{1\text{-}EEG}$ to $RESP_{EEG}$ for both awake ($dPTE$ = 0.089 bit, $p_{adj} < 0.001$) and sleep ($dPTE$ = 0.046 bit, $p_{adj} < 0.001$) (Fig. 3e). We found the drive of respiration by the $ISF_{1\text{-}EEG}$ phase decrease (Wilcoxon rank sum, FDR) during sleep ($\Delta dPTE$ = 0.043 bit, $p_{adj} < 0.001$, $Z = 4.352$) across the majority of the scalp (indicated by red areas), with no differences in frontal electrodes (Fig. 3f).

Taken together, these results confirmed our prediction that respiration phase would couple with cortical amplitudes extending from slow delta oscillations to the fast gamma range, and on a spatial scale even larger than for the ISF. We further showed, using directional metrics, that respiration phase also drives neuronal amplitudes. This was the first study to demonstrate that sleep state does not influence the coupling strength or mediate changes in net directionality between respiration and fast rhythms, despite respiration rhythm slowed down while showing increased spectral power.

4. Discussion

In this electrophysiological study of healthy humans across awake and sleeping states, we have uncovered multiple novel interactions with directional coupling, namely infra-slow physiological oscillations, respiration, and fast cortical activity. We established that the phases of ISFs and respiration were mutually coupled and together exhibited directional phase-amplitude modulation of the amplitudes of fast neuronal activities over a wide range of frequencies and cortical areas during wakefulness and sleep. The slow modulations of fast activities were independent of the power of the slow oscillations and were obtained through phase-amplitude coupling. Moreover, we found that a transition in arousal state from wakefulness to sleep was followed by lowered net drive of infra-slow phase. Our findings thus show that spontaneous brain activity is coordinated by the phases of respiration and infra-slow physiological oscillations in a manner dependent on the arousal state.

4.1. Infra-slow phase contributes to the drive of cortical excitability

A comparison of wakefulness and sleep conditions showed that ISF_{EEG} power increased during sleep, along with a concurrent reduction in fast oscillation amplitudes (see Fig. 1a). This increase of infraslow frequency power during sleep is in line with earlier observations (Helakari et al., 2022; Marshall et al., 1998, 1996). Previous work has indicated that ISF phase could be coupled at least locally with amplitudes of fast neuronal activities during detection-task performance (Monto et al., 2008) and during sleep (Vanhatalo et al., 2004), albeit based on studies with limited electrode coverage and cohort sizes. We herein used high-density 256-channel fbEEG in a group of 21 subjects to provide the most extensive view yet of ISF coupling in a direct comparison between sleep and waking states.

We found that fast oscillation amplitudes were phase-amplitude coupled with ISFs during wakefulness, and to an even great extent during sleep. For the first time, we showed that not only the magnitudes but also the spatial extent wherein ISF_{EEG} phase couples with fast neural oscillation amplitudes increased during sleep (see Fig. 1 b-c) via distinct coupling patterns (see Fig. 1 d). In conventional understanding, human sleep EEG is characterized by increased power of slow delta waves and the presence of sleep spindles occurring in the overlapping beta band (Erwin et al., 1984). In addition to these features of sleep, alpha rhythm can be suppressed during the period of drowsiness preceding sleep (Erwin et al., 1984). Interestingly, the most conspicuous of the present ISF phase-amplitude coupling changes occurred in these same frequency bands, all of which are well-linked to sleep, thus strengthening the association between ISFs and sleep.

While prior studies have demonstrated a phase-amplitude interaction of ISFs with fast neuronal activity, they relied upon correlative, undirected measures, which do not support the drawing of causal inferences. To resolve whether ISFs modulate the fast activities, or if ISFs are rather a consequence of the emergent slow dynamics of fast activities, we used a novel directional phase-amplitude coupling analysis. In this approach, phase transfer entropy (PTE) quantifies in a history-controlled manner the mutual

predictive powers of, respectively, ISF phase, and the amplitudes of fast neural rhythms. Using PTE, we found that the ISF_{EEG} phase was a robust driver of the amplitude fluctuations of fast oscillations. Moreover, this directional phase-amplitude coupling was frequency dependent, such that the slowest frequencies ($ISF_{1\text{-}EEG}$ > $ISF_{2\text{-}EEG}$ > $RESP_{EEG}$) were the strongest drivers.

One might reasonably expect the directional drive to be stronger during sleep than in wakefulness, given the precedents set by the circumstance of undirected phase-amplitude coupling and ISF power. Surprisingly, the present analysis revealed that net drive was lower in sleep. We deduced that an increased bidirectionality of the interaction between fast and infraslow oscillations would have a cancelling effect on the net drive. Nonetheless, prediction values dropped to a similar degree in both (fast → ISF & ISF → fast) directions during sleep (see Fig. 2a), with a reduced net drive, suggesting that the interaction does not become more bidirectional as compared to the awake state. We also showed that reduced ISF drive was not linearly related to phase locking (see Figure S4a) or autocorrelation (see Figure S5).

By exclusion, we suppose that the directed ISF drive may thus arise through mechanisms that are partially independent from the pathways that achieve the instantaneous, correlative phase-amplitude coupling and that establish the overall signal power levels. This proposal seems to require invoking a new model in which some undefined driver could coordinate the phase transitions both of ISF and fast neural oscillations during sleep. Such a model might necessarily require including additional factors such as brain water dynamics (Borchardt et al., 2021; Myllylä et al., 2018).

4.2. Respiration phase operates on wide spatial extent during wakefulness and sleep

Studies conducted several decades ago showed that responses in several brain regions to olfactory stimulus couple with nasal respiration (Adrian, 1942; Fontanini et al., 2003; Kay and Freeman, 1998). The first evidence of coupling between breathing and brain was found in mice during local field potential recordings (Biskamp et al., 2017; Ito et al., 2014; Yanovsky et al., 2014; Zhong et al., 2017). Fluctuations of brain activity co-varied with the respiratory envelope when monitored as oscillatory electrophysiological activity recorded using intracranial EEG (Herrero et al., 2018) and likewise in fMRI BOLD signals (Raitamaa et al., 2021). Furthermore, respiration phase and rate has been shown to couple with different brain regions during sleep in anesthetized mice (Girin et al., 2021; Hammer et al., 2021; Tort et al., 2021). Even though respiration have been studied extensively, only a few human studies have been conducted, exploring the effect of respiration to brain neuronal rhythm amplitude dynamics. During rest, Perl et al. (2019) discovered that respiration is accompanied by EEG changes linked to attention. Later, Kluger and Gross (2021) suggested that resting state MEG amplitudes are coupled across a wide range (2–150 Hz) by respiratory phase.

Considering the previous studies, it seems plausible that respiration has a role in organizing spontaneous brain activity. Still, there were hitherto no studies considering the effect of sleep on respiratory coupling with brain oscillations in humans. Present findings prompted us to delve deeper into the potential influence of respiration on neurophysiological rhythms, whether through direct or indirect means by affecting ISF drive. Our results suggest that the amplitude dynamics of fast neuronal activity are phase-amplitude coupled and are driven by the respiration phase of $RESP_{EEG}$, rather than exclusively by the phase of ISF_{EEG}. Interestingly, in contrast to ISF_{EEG}, the phase-amplitude coupling and directional drive did not exhibit significant differences between sleep and waking states. However, the transition from wakefulness to sleep revealed a link between respiratory rate and coupling strength, where slower breathing was associated with stronger coupling (see Figure S4c). These findings provide the initial evidence of respiration drive in human brain during sleep.

Previous work involving full night fMRI recordings showed that (<0.1 Hz) vasomotor waves increase in sleep (Chang et al., 2016; Liu et al., 2018). A recent ultrafast MREG BOLD study in humans indicated that increased EEG slow-wave power during sleep was accompanied with increased physiological brain pulsations, namely: vasomotor, respiratory and cardiovascular pulsations (Helakari et al., 2022). In the light of this, we suppose that the physiological pulsations could be linked to diurnal neurophysiological changes. The several physiological pulsations affecting both blood and cerebrospinal fluid (CSF) dynamics could in theory be a unifying external factor to explain the reduced drive of neuronal activity by the electrical gradient across the BBB during sleep, which is a matter requiring further investigation. As an index of BBB permeability (Nita et al., 2004; Voipio et al., 2003), EEG ISFs may emerge as an object of study in a variety of brain injury and disease contexts. The generalization of this concept calls for further investigation of ISF dynamics with cortical rhythms in various clinical conditions.

4.3. Limitations directing future work

Although our study design had limited recording time, we were able to make the most of the time we had available. We were able to record light sleep by using sleep deprivation to encourage sleep in the scanner, as demonstrated by the sleep scores in Table S1. For deeper sleep stages and rapid eye movement (REM) sleep, longer scan times would be required to achieve more comprehensive results. The awake and sleep scans were performed at different times of the day, such that circadian rhythms could have confounded the study. Additionally, after excluding various measurements, six of the 21 volunteers ended up providing unpaired measurements. We addressed this by using only unpaired statistical testing. Overall, we have leveraged these limitations to obtain valuable insights into the relationship between slow physiological and fast brain oscillations.

BBB permeability scans in conjunction with fbEEG recordings might eventually confirm the occurrence of change in hydrodynamics over BBB glia limitans in sleep. However, there is not yet any technology affording sufficiently fast recordings of BBB permeability changes across the sleep-wake cycle. Indeed, current experimental approaches are limited to invasive intracranial procedures, which are apt to perturb the flow of interstitial fluid and CSF (Plog et al., 2019; Shoffstall et al., 2018). The development of a non-invasive, multimodal neuroimaging method might eventually establish whether physiological CSF/blood pulsations are introducing hitherto undetected driving effects on sleep-related electrophysiological activity changes.

Acknowledgements

This work was funded by Jane & Aatos Erkko Foundation grants 1&210043 (V.Ki.), Academy of Finland Terva grants # 275342, 314497, 335720 (V.Ki), Aivosäätiö/BrainFoundation (J.K, V.Ki), Uniogs/MRC Oulu Doctoral Program-grant (H.H., J.K.), Pohjois-Suomen Terveydenhuollon tukisäätiö (H.H., V.Ko.), Instrumentarium Science Foundation (J.K), Emil Aaltonen Foundation (H.H, M.J), Finnish Medical Foundation (V.Ki., J.K., M.J.), VTR grants from Oulu University Hospital (V.Ki, V.Ko.), Finnish Neurological Foundation (V. Ki.), KEVO grants from Oulu University Hospital (V.Ki.), Orion Research Foundation (J.K.), Maire Taponen Foundation (J.K.). We acknowledge Inglewood Biomedical Editing for text revisions, Palva lab for providing a script for PTE calculation and CSC for com-

putational resources. We thank Jussi Kantola for data management and Annastiina Kivipää for assistance during measurements and volunteer recruitment.

Conflict of interest statement

The authors declare no conflicting interest.

Appendix A. Supplementary data

Supplementary data to this article can be found online at https://doi.org/10.1016/j.clinph.2023.10.013.

References

Adrian ED. Olfactory reactions in the brain of the hedgehog. J Physiol 1942;100:459–73. https://doi.org/10.1113/jphysiol.1942.sp003955.

Allen PJ, Josephs O, Turner R. A method for removing imaging artifact from continuous EEG recorded during functional MRI. Neuroimage 2000;12:230–9. https://doi.org/10.1006/nimg.2000.0599.

Allen PJ, Polizzi G, Krakow K, Fish DR, Lemieux L. Identification of EEG events in the MR scanner: the problem of pulse artifact and a method for its subtraction. Neuroimage 1998;8:229–39. https://doi.org/10.1006/nimg.1998.0361.

Arnulfo G, Wang SH, Myrov V, Toselli B, Hirvonen J, Fato MM, et al. Long-range phase synchronization of high-frequency oscillations in human cortex. Nat Commun 2020;11:5363. https://doi.org/10.1038/s41467-020-18975-8.

Benjamini Y, Hochberg Y. Controlling the False Discovery Rate: A Practical and Powerful Approach to Multiple Testing. J of the R Statistical Society Ser B (Methodological) 1995;57:289–300. https://doi.org/10.1111/j.2517-6161.1995.tb02031.x.

Besson JM, Woody CD, Aleonard P, Thompson HK, Albe-Fessard D, Marshall WH. Correlations of brain d-c shifts with changes in cerebral blood flow. Am J Physiol 1970;218:284–91. https://doi.org/10.1152/ajplegacy.1970.218.1.284.

Biskamp J, Bartos M, Sauer J-F. Organization of prefrontal network activity by respiration-related oscillations. Sci Rep 2017;7:45508. https://doi.org/10.1038/srep45508.

Borchardt V, Korhonen V, Helakari H, Nedergaard M, Myllylä T, Kiviniemi V. Inverse correlation of fluctuations of cerebral blood and water concentrations in humans. Eur Phys J Plus 2021;136:497. https://doi.org/10.1140/epjp/s13360-021-01480-2.

Bossomaier T, Barnett L, Harré M, Lizier JT. An Introduction to Transfer Entropy: Information Flow in Complex Systems. 1st ed. Springer International Publishing; 2016. https://doi.org/10.1007/978-3-319-43222-9.

Ceguerra R v., Lizier JT, Zomaya AY. Information storage and transfer in the synchronization process in locally-connected networks. 2011 IEEE Symposium on Artificial Life (ALIFE), IEEE; 2011, p. 54–61. https://doi.org/10.1109/ALIFE.2011.5954653.

Chang C, Leopold DA, Schölvinck ML, Mandelkow H, Picchioni D, Liu X, et al. Tracking brain arousal fluctuations with fMRI. Proc Natl Acad Sci U S A 2016;113:4518–23. https://doi.org/10.1073/pnas.1520613113.

Chaumon M, Bishop DVM, Busch NA. A practical guide to the selection of independent components of the electroencephalogram for artifact correction. J Neurosci Methods 2015;250:47–63. https://doi.org/10.1016/j.jneumeth.2015.02.025.

de Cheveigné A, Arzounian D. Robust detrending, rereferencing, outlier detection, and inpainting for multichannel data. Neuroimage 2018;172:903–12. https://doi.org/10.1016/j.neuroimage.2018.01.035.

Cohen MX. A better way to define and describe Morlet wavelets for time-frequency analysis. Neuroimage 2019;199:81–6. https://doi.org/10.1016/j.neuroimage.2019.05.048.

Cohen MX. Analyzing Neural Time Series Data. The MIT Press; 2014. https://doi.org/10.7551/mitpress/9609.001.0001.

Delorme A, Makeig S. EEGLAB: an open source toolbox for analysis of single-trial EEG dynamics including independent component analysis. J Neurosci Methods 2004;134:9–21. https://doi.org/10.1016/j.jneumeth.2003.10.009.

Erwin CW, Somerville ER, Radtke RA. A review of electroencephalographic features of normal sleep. J Clin Neurophysiol 1984;1:253–74. https://doi.org/10.1097/00004691-198407000-00001.

Flexman JE, Demaree RG, Simpson DD. Respiratory phase and visual signal detection. Percept Psychophys 1974;16:337–9. https://doi.org/10.3758/BF03203952.

Fontanini A, Spano P, Bower JM. Ketamine-xylazine-induced slow (< 1.5 Hz) oscillations in the rat piriform (olfactory) cortex are functionally correlated with respiration. J Neurosci 2003;23:7993–8001. https://doi.org/10.1523/JNEUROSCI.23-22-07993.2003.

Fritz CO, Morris PE, Richler JJ. Effect size estimates: Current use, calculations, and interpretation. J Exp Psychol Gen 2012;141:2–18. https://doi.org/10.1037/a0024338.

Fukunaga M, Horovitz SG, van Gelderen P, de Zwart JA, Jansma JM, Ikonomidou VN, et al. Large-amplitude, spatially correlated fluctuations in BOLD fMRI signals during extended rest and early sleep stages. Magn Reson Imaging 2006;24:979–92. https://doi.org/10.1016/j.mri.2006.04.018.

Fultz NE, Bonmassar G, Setsompop K, Stickgold RA, Rosen BR, Polimeni JR, et al. Coupled electrophysiological, hemodynamic, and cerebrospinal fluid oscillations in human sleep. Science 2019;366:628–31. https://doi.org/10.1126/science.aax5440.

Girin B, Juventin M, Garcia S, Lefèvre L, Amat C, Fourcaud-Trocmé N, et al. The deep and slow breathing characterizing rest favors brain respiratory-drive. Sci Rep 2021;11:7044. https://doi.org/10.1038/s41598-021-86525-3.

Hammer M, Schwale C, Brankačk J, Draguhn A, Tort ABL. Theta-gamma coupling during REM sleep depends on breathing rate. Sleep 2021;44. https://doi.org/10.1093/sleep/zsab189.

Helakari H, Korhonen V, Holst SC, Piispala J, Kallio M, Väyrynen T, et al. Human NREM Sleep Promotes Brain-Wide Vasomotor and Respiratory Pulsations. J Neurosci 2022;42:2503–15. https://doi.org/10.1523/JNEUROSCI.0934-21.2022.

Held D, Fencl V, Pappenheimer JR. Electrical potential of cerebrospinal fluid. J Neurophysiol 1964;27:942–59. https://doi.org/10.1152/jn.1964.27.5.942.

Herrero JL, Khuvis S, Yeagle E, Cerf M, Mehta AD. Breathing above the brain stem: volitional control and attentional modulation in humans. J Neurophysiol 2018;119:145–59. https://doi.org/10.1152/jn.00551.2017.

Hiltunen T, Kantola J, Abou Elseoud A, Lepola P, Suominen K, Starck T, et al. Infra-Slow EEG Fluctuations Are Correlated with Resting-State Network Dynamics in fMRI. J Neurosci 2014;34:356–62. https://doi.org/10.1523/JNEUROSCI.0276-13.2014.

Horovitz SG, Braun AR, Carr WS, Picchioni D, Balkin TJ, Fukunaga M, et al. Decoupling of the brain's default mode network during deep sleep. Proc Natl Acad Sci U S A 2009;106:11376–81. https://doi.org/10.1073/pnas.0901435106.

Hughes SW, Lőrincz ML, Parri HR, Crunelli V. Infra-slow (<0.1 Hz) oscillations in thalamic relay nuclei: basic mechanisms and significance to health and disease states. Prog Brain Res, vol. 193, Elsevier; 2011, p. 145–62. https://doi.org/10.1016/B978-0-444-53839-0.00010-7.

Huigen E, Peper A, Grimbergen C. Investigation into the origin of the noise of surface electrodes. Med Biol Eng Comput 2002;40:332–8. https://doi.org/10.1007/BF02344216.

Hyvarinen A. Fast and robust fixed-point algorithms for independent component analysis. IEEE Trans Neural Netw 1999;10:626–34. https://doi.org/10.1109/72.761722.

Ito J, Roy S, Liu Y, Cao Y, Fletcher M, Lu L, et al. Whisker barrel cortex delta oscillations and gamma power in the awake mouse are linked to respiration. Nat Commun 2014;5:3572. https://doi.org/10.1038/ncomms4572.

Johannknecht M, Kayser C. The influence of the respiratory cycle on reaction times in sensory-cognitive paradigms. Sci Rep 2022;12:2586. https://doi.org/10.1038/s41598-022-06364-8.

Kananen J, Helakari H, Korhonen V, Huotari N, Järvelä M, Raitamaa L, et al. Respiratory-related brain pulsations are increased in epilepsy—a two-centre functional MRI study. Brain Commun 2020;2:fcaa076. https://doi.org/10.1093/braincomms/fcaa076.

Kananen J, Järvelä M, Korhonen V, Tuovinen T, Huotari N, Raitamaa L, et al. Increased interictal synchronicity of respiratory related brain pulsations in epilepsy. J Cereb Blood Flow Metab 2022;42:1840–53. https://doi.org/10.1177/0271678X221099703.

Kaufmann C, Wehrle R, Wetter TC, Holsboer F, Auer DP, Pollmächer T, et al. Brain activation and hypothalamic functional connectivity during human non-rapid eye movement sleep: an EEG/fMRI study. Brain 2006;129:655–67. https://doi.org/10.1093/brain/awh686.

Kay LM, Freeman WJ. Bidirectional processing in the olfactory-limbic axis during olfactory behavior. Behav Neurosci 1998;112:541–53. https://doi.org/10.1037/0735-7044.112.3.541.

Keinänen T, Rytky S, Korhonen V, Huotari N, Nikkinen J, Tervonen O, et al. Fluctuations of the EEG-fMRI correlation reflect intrinsic strength of functional connectivity in default mode network. J Neurosci Res 2018;96:1689–98. https://doi.org/10.1002/jnr.24257.

Kiviniemi V, Korhonen V, Kortelainen J, Rytky S, Keinänen T, Tuovinen T, et al. Real-time monitoring of human blood-brain barrier disruption. PLoS One 2017;12:e0174072.

Kluger DS, Gross J. Respiration modulates oscillatory neural network activity at rest. PLoS Biol 2021;19:e3001457. https://doi.org/10.1371/journal.pbio.3001457.

Korhonen V, Hiltunen T, Myllylä T, Wang X, Kantola J, Nikkinen J, et al. Synchronous Multiscale Neuroimaging Environment for Critically Sampled Physiological Analysis of Brain Function: Hepta-Scan Concept. Brain Connect 2014;4:677–89. https://doi.org/10.1089/brain.2014.0258.

Lachaux J-P, Rodriguez E, Martinerie J, Varela FJ. Measuring phase synchrony in brain signals. Hum Brain Mapp 1999;8:194–208. https://doi.org/10.1002/(SICI)1097-0193(1999)8:4<194::AID-HBM4>3.0.CO;2-C.

Leopold DA, Murayama Y, Logothetis NK. Very slow activity fluctuations in monkey visual cortex: implications for functional brain imaging. Cereb Cortex 2003;13:422–33. https://doi.org/10.1093/cercor/13.4.422.

Li S, Rymer WZ. Voluntary Breathing Influences Corticospinal Excitability of Nonrespiratory Finger Muscles. J Neurophysiol 2011;105:512–21. https://doi.org/10.1152/jn.00946.2010.

Liu X, de Zwart JA, Schölvinck ML, Chang C, Ye FQ, Leopold DA, et al. Subcortical evidence for a contribution of arousal to fMRI studies of brain activity. Nat Commun 2018;9:395. https://doi.org/10.1038/s41467-017-02815-3.

Lobier M, Siebenhühner F, Palva S, Matias PJ. Phase transfer entropy: A novel phase-based measure for directed connectivity in networks coupled by oscillatory

interactions. Neuroimage 2014;85:853–72. https://doi.org/10.1016/j.neuroimage.2013.08.056.
Marshall L, Mölle M, Fehm HL, Born J. Scalp recorded direct current brain potentials during human sleep. Eur J Neurosci 1998;10:1167–78. https://doi.org/10.1046/j.1460-9568.1998.00131.x.
Marshall L, Molle M, Michaelsen S, Fehm HL, Born J. Slow potential shifts at sleep–wake transitions and shifts between NREM and REM sleep. Sleep 1996;19:145–51. https://doi.org/10.1093/sleep/19.2.145.
Monto S, Palva S, Voipio J, Palva JM. Very Slow EEG Fluctuations Predict the Dynamics of Stimulus Detection and Oscillation Amplitudes in Humans. J Neurosci 2008;28:8268–72. https://doi.org/10.1523/JNEUROSCI.1910-08.2008.
Myllylä T, Harju M, Korhonen V, Bykov A, Kiviniemi V, Meglinski I. Assessment of the dynamics of human glymphatic system by near-infrared spectroscopy. J Biophotonics 2018:11. https://doi.org/10.1002/jbio.201700123.
Niedermeyer E, Lopes da Silva, Fernando H, Donald L. Schomer, Vanhatalo S, Voipio J, et al. Electroencephalography: Basic principles, clinical applications, and related fields. vol. 6. 6th ed. Wolters Kluwer Health/Lippincott Williams & Wilkins; 2011.
Nikulin VV, Fedele T, Mehnert J, Lipp A, Noack C, Steinbrink J, et al. Monochromatic Ultra-Slow (∼0.1Hz) Oscillations in the human electroencephalogram and their relation to hemodynamics. Neuroimage 2014;97:71–80. https://doi.org/10.1016/j.neuroimage.2014.04.008.
Nita DA, Vanhatalo S, Lafortune F-D, Voipio J, Kaila K, Amzica F. Nonneuronal origin of CO2-related DC EEG shifts: an in vivo study in the cat. J Neurophysiol 2004;92:1011–22. https://doi.org/10.1152/jn.00110.2004.
Nunez PL, Srinivasan R, Westdorp AF, Wijesinghe RS, Tucker DM, Silberstein RB, et al. EEG coherency: I: statistics, reference electrode, volume conduction, Laplacians, cortical imaging, and interpretation at multiple scales. Electroencephalogr Clin Neurophysiol 1997;103:499–515. https://doi.org/10.1016/S0013-4694(97)00066-7.
Palva JM, Palva S. Infra-slow fluctuations in electrophysiological recordings, blood-oxygenation-level-dependent signals, and psychophysical time series. Neuroimage 2012;62:2201–11. https://doi.org/10.1016/j.neuroimage.2012.02.060.
Palva JM, Palva S, Kaila K. Phase synchrony among neuronal oscillations in the human cortex. J Neurosci 2005;25:3962–72. https://doi.org/10.1523/JNEUROSCI.4250-04.2005.
Palva JM, Zhigalov A, Hirvonen J, Korhonen O, Linkenkaer-Hansen K, Palva S. Neuronal long-range temporal correlations and avalanche dynamics are correlated with behavioral scaling laws. Proc Natl Acad Sci U S A 2013;110:3585–90. https://doi.org/10.1073/pnas.1216855110.
Perl O, Ravia A, Rubinson M, Eisen A, Soroka T, Mor N, et al. Human non-olfactory cognition phase-locked with inhalation. Nat Hum Behav 2019;3:501–12. https://doi.org/10.1038/s41562-019-0556-z.
Plog BA, Lou N, Pierre CA, Cove A, Kenney HM, Hitomi E, et al. When the air hits your brain: decreased arterial pulsatility after craniectomy leading to impaired glymphatic flow. J Neurosurg 2019:1–14. https://doi.org/10.3171/2019.2.JNS182675.
Raitamaa L, Huotari N, Korhonen V, Helakari H, Koivula A, Kananen J, et al. Spectral analysis of physiological brain pulsations affecting the BOLD signal. Hum Brain Mapp 2021;42:4298–313. https://doi.org/10.1002/hbm.25547.
Scott DW. On optimal and data-based histograms. Biometrika 1979;66:605–10. https://doi.org/10.1093/biomet/66.3.605.
Shoffstall AJ, Paiz JE, Miller DM, Rial GM, Willis MT, Menendez DM, et al. Potential for thermal damage to the blood–brain barrier during craniotomy: implications for intracortical recording microelectrodes. J Neural Eng 2018;15. https://doi.org/10.1088/1741-2552/aa9f32 034001.
Theiler J, Eubank S, Longtin A, Galdrikian B, Doyne FJ. Testing for nonlinearity in time series: the method of surrogate data. Physica D 1992;58:77–94. https://doi.org/10.1016/0167-2789(92)90102-S.
Timme NM, Lapish C. A Tutorial for Information Theory in Neuroscience. ENeuro 2018:5. https://doi.org/10.1523/ENEURO.0052-18.2018.
Tort ABL, Hammer M, Zhang J, Brankačk J, Draguhn A. Temporal Relations between Cortical Network Oscillations and Breathing Frequency during REM Sleep. J Neurosci 2021;41:5229–42. https://doi.org/10.1523/JNEUROSCI.3067-20.2021.
Tschirgi RD, Taylor JL. Slowly Changing Bioelectric Potentials Associated With the Blood-Brain Barrier. Am J Physiol 1958;195:7–22. https://doi.org/10.1152/ajplegacy.1958.195.1.7.
Vanhatalo S, Palva JM, Holmes MD, Miller JW, Voipio J, Kaila K. Infraslow oscillations modulate excitability and interictal epileptic activity in the human cortex during sleep. Proc Natl Acad Sci U S A 2004;101:5053–7. https://doi.org/10.1073/pnas.0305375101.
Voipio J, Tallgren P, Heinonen E, Vanhatalo S, Kaila K. Millivolt-Scale DC Shifts in the Human Scalp EEG: Evidence for a Nonneuronal Generator. J Neurophysiol 2003;89:2208–14. https://doi.org/10.1152/jn.00915.2002.
Watson BO. Cognitive and Physiologic Impacts of the Infraslow Oscillation. Front Syst Neurosci 2018:12. https://doi.org/10.3389/fnsys.2018.00044.
Yanovsky Y, Ciatipis M, Draguhn A, Tort ABL, Brankačk J. Slow Oscillations in the Mouse Hippocampus Entrained by Nasal Respiration. J Neurosci 2014;34:5949–64. https://doi.org/10.1523/JNEUROSCI.5287-13.2014.
Zelano C, Jiang H, Zhou G, Arora N, Schuele S, Rosenow J, et al. Nasal Respiration Entrains Human Limbic Oscillations and Modulates Cognitive Function. J Neurosci 2016;36:12448–67. https://doi.org/10.1523/JNEUROSCI.2586-16.2016.
Zhong W, Ciatipis M, Wolfenstetter T, Jessberger J, Müller C, Ponsel S, et al. Selective entrainment of gamma subbands by different slow network oscillations. Proc Natl Acad Sci U S A 2017;114:4519–24. https://doi.org/10.1073/pnas.1617249114.